Heat transfer and frictional pressure drop during condensation in plate heat exchangers Assessment of correlations and a new method

Tao, Xuan; Infante Ferreira, Carlos A.

DOI
10.1016/j.ijheatmasstransfer.2019.01.132

Publication date
2019

Document Version
Final published version

Published in
International Journal of Heat and Mass Transfer

International Journal of Heat and Mass Transfer 135 (2019) 996–1012

Contents lists available at ScienceDirect

International Journal of Heat and Mass Transfer

journal homepage: www.elsevier.com/locate/ijhmt

Review

Heat transfer and frictional pressure drop during condensation in plate heat exchangers: Assessment of correlations and a new method

Xuan Tao *, Carlos A. Infante Ferreira

Process and Energy Laboratory, Delft University of Technology, Leeghwaterstraat 39, 2628 CB Delft, the Netherlands

ARTICLE INFO

Article history:
Received 29 September 2018
Received in revised form 11 January 2019
Accepted 28 January 2019

Keywords:
Condensation heat transfer
Two-phase frictional pressure drop
Assessment
Multi-variable regression analysis
Plate heat exchangers

ABSTRACT

The corrugation channels of plate heat exchangers enhance the heat transfer and complicate the prediction of heat transfer coefficients and frictional pressure drop. This paper reviews the heat transfer and frictional pressure drop correlations for condensation in plate heat exchangers, and classifies the correlations into basic forms. An experimental database is developed including the data of HFCs, hydrocarbons, HFOs and CO_2. The mass fluxes are in the range of 2–150 $kg{\cdot}m^{-2}{\cdot}s^{-1}$. The chevron angles and hydraulic diameters are distributed in 25.7°–70° and 3.23–8.08 mm. The saturated temperatures are −34.4 to 72.1 °C, while the reduced pressures are from 0.03 to 0.49. Eight heat transfer correlations are assessed with the database. The correlation of Longo et al. [48] predicts the experimental data best, while the correlation of Kuo et al. [16] shows the second best performance. Six frictional pressure drop correlations are compared with the database. The prediction of frictional pressure drop is relatively poor, and a new correlation is developed using multi-variable regression analysis with non-dimensional numbers. This new correlation predicts 87.5% of the experimental data within ±50%.

Contents

1. Introduction . . . 997
2. Non-dimensional numbers used in condensation . . . 998
   2.1. Fluid properties of two-phase flow . . . 998
   2.2. Forces in condensing flow . . . 998
   2.3. Heat flux, sensible heat and latent heat . . . 999
3. Summary of experimental database . . . 999
4. Heat transfer correlations . . . 999
   4.1. Nusselt correlation . . . 1002
   4.2. Akers correlation . . . 1002
   4.3. Webb correlation . . . 1002
   4.4. Shah correlation . . . 1002
   4.5. Mancin correlation . . . 1003
   4.6. Wang correlation . . . 1003
   4.7. Winkelmann correlation . . . 1003
   4.8. Correlation for mixtures . . . 1003
5. Assessment of heat transfer correlations . . . 1004
6. Frictional pressure drop correlations . . . 1006
   6.1. Two-phase Fanning friction factor . . . 1006
   6.2. Lockhart-Martinelli model . . . 1007
   6.3. Kinetic energy model . . . 1007

* Corresponding author.
E-mail addresses: x.tao@tudelft.nl (X. Tao), c.a.infanteferreira@tudelft.nl (C.A. Infante Ferreira).

https://doi.org/10.1016/j.ijheatmasstransfer.2019.01.132
0017-9310/

Nomenclature

Symbols

Bd	Bond number [–]
Bo	Boiling number [–]
Co	Convection number [–]
c_p	specific heat [J kg^{-1} K^{-1}]
d_e	equivalent diameter [m]
d_h	hydraulic diameter [m]
f	friction factor [–]
Fr	Froude number [–]
g	gravitational constant [ms^{-2}]
G	mass flux [kg m^{-2} s^{-1}]
Ga	Galileo number [–]
h	enthalpy [J kg^{-1}]
Ja	Jakob number [–]
j_G	non-dimensional gas velocity Eq. (46) [–]
k_i	parameter defined in Eq. (79) [–]
KE/V	kinetic energy per unit volume [J m^{-3}]
L_p	port-to-port plate length [m]
m_i	parameter defined in Eq. (79) [–]
n_i	parameter defined in Eq. (79) [–]
Nu	Nusselt number [–]
P	pressure [Pa]
Pr	Prandtl number [–]
$\dot{q}$	heat flux [W m^{-2}]
Re	Reynolds number [–]
T	temperature [K]
v	superficial velocity [m s^{-1}]
We	Weber number [–]
W_p	port-to-port plate width [m]
x	vapor quality [–]
X	Lockhart-Martinelli parameter [–]

Greek symbols

α	heat transfer coefficient [W m^{-2} K^{-1}]
β	chevron angle to flow direction [°]
Δ	difference [–]
δ	surface roughness [m]
ε	void fraction [–]
Θ_i	parameter defined in Eq. (79) [–]
ϕ	surface enlargement factor [–]
ϕ_L	two-phase friction factor [–]
ζ	parameter defined in Eq. (77) [–]
λ	thermal conductivity [W m^{-1} K^{-1}]
Λ_{wave}	corrugation wavelength [m]
μ	dynamic viscosity [Pa s]
ρ	density [kg m^{-3}]
σ	surface tension [N m^{-1}]

Subscripts

av	averaged
c	combined or transitional condensation
cc	convective condensation
cr	critical conditions
de	deceleration
ele	elevation
eq	equivalent
exp	experimental data
fri	frictional pressure drop
G	gas or vapor
gc	gravity-controlled condensation
$high$	high limit
$homo$	homogeneous flow
in_port	inlet port of test section
L	liquid
LG	latent liquid to vapor
LO	liquid only
low	low limit
max	the maximum value
mea	measurement
mix	mixture
mod	modified
out_port	outlet port of test section
pre	predicted data
$pure$	pure fluid
sat	at saturation conditions
sup	superheating
TP	two-phase
tt	turbulent-turbulent flow
$wall$	at wall conditions

7. Assessment of frictional pressure drop correlations . . . 1007
8. A new frictional pressure drop correlation . . . 1009
9. Conclusions . . . 1011
Conflict of interest . . . 1011
Acknowledgements . . . 1011
References . . . 1011

1. Introduction

Plate heat exchangers (PHEs) have gained increasing applications with single-phase and two-phase in recent decades. A PHE is composed of a stack of plates, which usually have sinusoidal corrugations. A flow channel is formed by two adjacent plates. The complex structure of the channel contributes to disturbances in the flow and improves heat transfer performance [1,2,3].

PHEs are promising candidates for condensation processes since their geometries tend to break up the condensate and enhance the heat transfer. During condensation, heat transfer and frictional pressure drop are influenced by mass flux, vapor quality, heat flux, condensation pressure, superheating, fluid properties and plate geometries [4]. Several experiments have been carried out on condensation, resulting in heat transfer and frictional pressure drop correlations.

Thonon et al. [5] discussed the design of PHEs used for single-phase heat transfer, evaporation and condensation. Single-phase heat transfer is deteriorated in the downstream areas of the corrugation edges because of recirculation. During evaporation, the critical vapor quality of dryout is lower for PHEs than for smooth geometries, which is attributed to the fact that the corrugation washes the liquid film out from the wall. This structure seems to promote the drainage of condensate and improve heat transfer.

García-Cascales et al. [6] summarized the heat transfer correlations of single-phase, evaporation and condensation. The Akers et al. [7] correlation is widely adopted by adding non-dimensional fluid properties or geometric parameters. The correlations of evaporation and condensation include heat flux and vapor quality, and are compared with experimental data. In general, the evaporation correlations predict the experimental data better than the condensation correlations.

Amalfi et al. [8,9] collected the experimental data of flow boiling in PHEs, including 1903 heat transfer and 1513 frictional pressure drop data. The database was used to develop new heat transfer and frictional pressure drop correlations by dimensional analysis coupled with multi-variable regression analysis, whose predicting performance is satisfactory. Similar analysis was carried out on the condensation within PHEs, and eight heat transfer correlations were compared with 325 experimental data [10]. The selected correlations did not perform well, but no new correlation was proposed.

Eldeeb et al. [11] surveyed the heat transfer and frictional pressure drop correlations of evaporation and condensation, and calculated the heat transfer coefficients (HTCs) of several refrigerants. Research on condensation is less than on evaporation. The predictions of these correlations are considerably different, and need to be validated. Despite the growing need for accurate prediction, the available simulation tools of PHEs are limited.

Most heat transfer and frictional pressure drop correlations are applicable in the original operating ranges of the condensation experiments, but the predicting performance is unknown outside that range. Widely applicable and accurate correlations are needed. This paper aims to provide suitable methods to calculate heat transfer and frictional pressure drop. It summarizes condensation correlations in PHEs, and develops an experimental database. The correlations are assessed by comparison with the database. Section 2 lists non-dimensional numbers used to describe two-phase flow. Section 3 builds an experimental database of heat transfer and frictional pressure drop. In Section 4, several heat transfer correlations are considered, and are compared with the database in Section 5. Frictional pressure drop correlations are classified into basic forms in Section 6, and are assessed with the database in Section 7. Since the data are not well predicted, Section 8 develops a new frictional pressure drop correlation and gives a cross validation.

2. Non-dimensional numbers used in condensation

Several non-dimensional numbers are used in the heat transfer and frictional pressure drop correlations. For the convenience of discussion, this section lists these numbers and distinguishes between similar definitions.

2.1. Fluid properties of two-phase flow

The Lockhart-Martinelli parameter, X, describes the separated two-phase flow of four combinations: turbulent liquid and turbulent vapor, laminar liquid and turbulent vapor, turbulent liquid and laminar vapor, as well as laminar liquid and laminar vapor [12]. In the case of turbulent liquid and turbulent vapor, X_{tt} is calculated with Eq. (1) [13].

$$X_{tt} = \left(\frac{1-x}{x}\right)^{0.9}\left(\frac{\rho_G}{\rho_L}\right)^{0.5}\left(\frac{\mu_L}{\mu_G}\right)^{0.1} \tag{1}$$

Eq. (2) defines the Convection number, which mainly indicates the influence of vapor quality [14,15]. Kuo et al. [16] calculated the Convection number differently as given in Eq. (3).

$$Co = \left(\frac{\rho_G}{\rho_L}\right)^{0.5}\left(\frac{1-x}{x}\right)^{0.8} \tag{2}$$

$$Co_2 = \left(\frac{\rho_G}{\rho_L}\right)\left(\frac{1-x}{x}\right)^{0.8} \tag{3}$$

The averaged density is calculated by assuming homogeneous flow at the averaged vapor quality. The two-phase flow is treated as a single fluid.

$$\frac{1}{\rho_{av}} = \frac{1-x_{av}}{\rho_L} + \frac{x_{av}}{\rho_G} \tag{4}$$

The Prandtl number is used to predict the HTC during convective condensation. The value of liquid phase is usually taken since the heat passes through the condensate film:

$$Pr_L = \frac{c_{p,L}\mu_L}{\lambda_L} \tag{5}$$

2.2. Forces in condensing flow

The Reynolds number is the ratio of inertia to viscous forces and has different forms including Re_{eq}, Re_{LO}, Re_L and Re_G. Eq. (6) gives the equivalent Reynolds number of two-phase flow, Re_{eq}, which is more relevant for homogeneous flow. G is the mass flux and d_h is the hydraulic diameter. The liquid only Reynolds number, Re_{LO}, in Eq. (7) is defined by assuming all the fluid is liquid. Re_{LO} is used to calculate the liquid only HTC. Eq. (8) defines the liquid Reynolds number, Re_L, which is also known as the condensate Reynolds number. Re_L only considers the mass flux of liquid phase. Similarly, the vapor Reynolds number, Re_G, in Eq. (9) focuses on the mass flux of vapor phase. Eqs. (6)–(9) use the dynamic viscosities of liquid or vapor. In Eq. (10), the modified Reynolds number, $Re_{\ mod}$, includes the averaged dynamic viscosity instead [17].

$$Re_{eq} = \frac{G[(1-x)+x(\rho_L/\rho_G)^{0.5}]d_h}{\mu_L} \tag{6}$$

$$Re_{LO} = \frac{Gd_h}{\mu_L} \tag{7}$$

$$Re_L = \frac{G_L d_h}{\mu_L} = \frac{G(1-x)d_h}{\mu_L} \tag{8}$$

$$Re_G = \frac{G_G d_h}{\mu_G} = \frac{Gxd_h}{\mu_G} \tag{9}$$

$$Re_{\ mod} = \frac{Gd_h}{\left(\frac{1-x_{av}}{\mu_L}+\frac{x_{av}}{\mu_G}\right)^{-1}} \tag{10}$$

The Weber number is the ratio of inertia to surface tension. Eq. (11) applies for the liquid phase. In Eq. (12), the homogeneous Weber number, We_{homo}, is calculated from the averaged density [9,18].

$$We_L = \frac{\rho_L v_L^2 d_h}{\sigma} = \frac{G^2(1-x)^2 d_h}{\rho_L \sigma} \tag{11}$$

$$We_{\mathrm{homo}} = \frac{\rho_{av} v_{av}^2 d_h}{\sigma} = \frac{G^2 d_h}{\rho_{av}\sigma} \tag{12}$$

The Froude number is the ratio of inertia to gravity, and is used by Kuo et al. [16] in the form of Eq. (13).

$$Fr_L = \frac{G^2}{\rho_L^2 g d_h} \tag{13}$$

The Galileo number, *Ga*, represents the ratio of gravity to viscous force and is defined in Eq. (14) [19].

$$Ga = \frac{\rho_L(\rho_L - \rho_G)gd_h^3}{\mu_L^2} \tag{14}$$

The Bond number, *Bd*, indicates the ratio of buoyancy to surface tension and distinguishes macroscale and microscale during two-phase flow [9].

$$Bd = \frac{(\rho_L - \rho_G)gd_h^2}{\sigma} \tag{15}$$

2.3. Heat flux, sensible heat and latent heat

The Boiling number, *Bo*, is the non-dimensional heat flux and is defined in Eq. (16), where Δh_{LG} is the latent heat [20,16]. The equivalent Boiling number is given in Eq. (17) [21,22].

$$Bo = \frac{\dot{q}}{G\Delta h_{LG}} \tag{16}$$

$$Bo_{eq} = \frac{\dot{q}}{G[(1-x) + x(\rho_L/\rho_G)^{0.5}]\Delta h_{LG}} \tag{17}$$

Eq. (18) indicates the influence of condensate film on heat transfer [23]. Δh_{LG} is added with the sensible heat of the liquid film because the condensate is subcooled. This parameter is referred to as the Jakob number, *Ja* [17,24].

$$Ja = \frac{c_{p,L}(T_{sat} - T_{wall})}{\Delta h_{LG} + 0.68c_{p,L}(T_{sat} - T_{wall})} \tag{18}$$

3. Summary of experimental database

In order to assess the correlations of heat transfer and frictional pressure drop in available literature, this section develops an experimental database and gives a summary in Table 1. Only condensation experiments are involved, and the flow is always vertical downward. There are 2376 heat transfer data and 1590 frictional pressure drop data. The test sections are brazed plate heat exchangers (BPHEs) or gasketed plate heat exchangers (GPHEs). For circular shell and plate heat exchangers (SPHEs), the heat transfer and flow characteristics are expected to be different due to the circular plates [25]. Most data were determined by overall measurements, while local HTCs were also measured [26,15,27,28,21,29]. The composition of the heat transfer database is further presented in Fig. 1. The working fluids are pure refrigerants (HFCs, hydrocarbons, HFOs and CO_2), near-azeotropic mixtures (R410A and R404A) and one zeotropic mixture (R407C). R134a and R410A account for approximately half of the database. Data for ammonia are not available. The classifications of chevron angles and hydraulic diameters are discrete, spanning the ranges of 25.7°–70° and 3.2–8.1 mm, respectively. The mass fluxes are from 0 to 150 $kg{\cdot}m^{-2}{\cdot}s^{-1}$, and mostly have small and intermediate values. The saturated temperatures are mostly concentrated in 20–40 °C. All the data below 0 °C are from the condensation of CO_2 [24]. The reduced pressures are nearly evenly distributed from 0 to 0.5.

Most inlet conditions are saturated two-phase or superheated vapor, while the outlets are saturated two-phase or subcooled liquid. Some of the inlets and outlets are controlled to be saturated vapor and saturated liquid, respectively [29,30]. In terms of superheating and subcooling, some research assumed that single-phase regions for de-superheating or subcooling do not appear, and used the saturated temperature for data reduction [31–36]. However, Hayes et al. [24,37] predicted the areas of de-superheating and subcooling regions using single-phase HTCs, and calculated the HTCs and frictional pressure drop for two-phase region. Local measurements determined the starting and ending points of condensation directly, allowing the calculation of the local HTCs [26,15,27,28,21].

In fact, at the superheated inlets, when the wall temperature is below the saturated temperature, the vapor starts to condensate directly without specific vapor regions [38]. The heat flux is transferred for phase change and de-superheating simultaneously [39]. The appearance of vapor regions is determined by the superheating degree, mass fluxes and heat fluxes. The onset of condensation happens earlier when the mass flux is smaller and the heat flux is larger [40,41]. When the condensers were connected with compressors, the superheating was significant, and the vapor regions were excluded by local measurements [27,28,21]. According to the infrared measurement of Sarraf et al. [39], the areas of de-superheating regions decreased when the superheating degree was decreased. Based on calculation, Mancin et al. [36] claimed that the vapor region did not appear for their experimental data since the wall temperature was below the saturated temperature.

The subcooling at the outlet is less investigated. Since the liquid film is subcooled by the wall, vapor phase remains present when the bulk vapor quality becomes 0 [40]. The appearance of liquid regions is expected to depend on the subcooling degree. The experiments of Longo [31–33] had small subcooling degrees, and the author assumed that there was no liquid region. Zhang et al. [18] and Sarraf et al. [39] considered the de-superheating and saturated regions as a whole, but subtracted the subcooling region.

To compare the correlations with the experimental data in Sections 5 and 7, assumptions are made if operating parameters are not clearly reported in the original papers. In PHEs, the vapor quality usually changes largely because of the small mass fluxes and large heat transfer areas. The averaged vapor qualities of the inlet and outlet represent the operating conditions. In the papers, both actual heat transfer areas and projected heat transfer areas are used during data reduction. The present database conforms the HTCs to the values based on actual heat transfer areas, so the experimental data can be compared with the correlations. Some of the geometric parameters are missing and are calculated according to the equations in Tao et al. [4]. Most fluid properties are determined using Refprop 9.1 [42], while R1234ze(Z) and R1233zd(E) are not included in this version and need other Refs. [43,44,45,46]. Most of the frictional pressure drop data are collected under the same operating conditions as for heat transfer.

4. Heat transfer correlations

Tao et al. [4] reviewed the condensation mechanisms in PHEs. In gravity-controlled regime, according to Nusselt's theory, the thickness of the condensate film increases with mass flux and deteriorates the heat transfer. In fact, the waves at the condensate surface cannot be eliminated, and the HTCs may stay constant. Convective condensation is mainly governed by interfacial shear, where HTCs mostly increase with mass flux. The transition of the condensation mechanisms is primarily contributed by mass flux and vapor quality. Higher vapor quality exerts a positive influence on heat transfer for most refrigerants, except for steam [23].

Condensation heat transfer correlations from different groups are summarized in this section, which calculate the HTCs based on actual heat transfer areas unless otherwise explained. All the correlations predict the averaged HTCs except for Shi et al. [21]. The correlations are classified by the basic forms that were firstly presented or widely accepted. Some of them are developed by modifying the basic forms.

Table 1
Experimental database of heat transfer and frictional pressure drop for condensation in plate heat exchangers.

Study	Test section		Refrigerants	$d_h/d_e/\beta/\Lambda_{wave}$[a]	L_p/W_p	T_{sat}	P_{sat}	G	x	Inlet and outlet[b]	$\dot{q}$	N_{HT}/N_{PD}[c]
	Type	Channels[d]		[mm/mm/-/mm]	[mm/mm]	[°C]	[bar]	[$kgm^{-2}s^{-1}$]	[-]		[kWm^{-2}]	
Sarraf et al. [26,39]	BPHE	1/1	R601	3.44/4.4/55°/6	476/111.4	36.5	1.0	9~29.8	0~1	SHV/SCL	20~66.5	144/24
Winkelmann [15]	GPHE	1/2[e]	R134a	4.65/6/25.7°/9.32	400/160	28.2~39.9	7.3~10.1	63	0~1	SHV/TP	6.9~51	111/41
Han et al. [50]	BPHE	2/3	R410A	3.68/4.3/45°/7 3.68/4.3/55°/5.2 3.68/4.3/70°/4.9	478/115	20~30	14.4~18.9	13~34	0.15~0.9	TP/TP	4.7~5.3	58/58
Longo et al. [31–33,48,58–74]	BPHE	4/5	R236fa,R134a,R410A, R152a,R404A, R600a, R290,R1270,R1234yf, R1234ze(E), R1234ze(Z)	3.23/4/65°/8	278/72	25~40	2.1~24.2	5~45	0~1	SHV/SCL TP/TP	5~25	823/528
Grabenstein and Kabelac [29]	GPHE	-	R134a	5.19/6/63°/11.4	368/408	11.1~23.7	4.3~6.4	30~74	0~1	SV/SL	8.5~17.6	42/19
Kabelac and Freund [27] Djordjevic et al. [28] Shi et al. [21]	GPHE	4/5	R134a	5.52/6.4/63.3°/12	1092/486	16.2~29	5.1~7.5	22~65	0~1	SHV/SCL	11.5~35	200/184
Hayes et al. [24,37]	BPHE	1/2	CO_2	3.33/4/30°/- 3.33/4/30°~63°/- 3.33/4/63°/-	444.5/127	-34.4~-17.8	1.2~2.1	2~45	0~1	SHV/SCL	2.5~15.7	98/83
Yan et al. [20] Kuo et al. [16]	BPHE	1/1	R134a, R410A	3.38/5.8/60°/10	450/120	19.9~35.5	7~19.5	50~150	0.1~0.9	TP/TP	10~20	228/227
Mancin et al. [34–36]	BPHE	1/2 3/4 2/3	R407C, R410A, R32	-/-/65°/-	487/247 325/94 526/111	36.5~41.8	16.1~22.7	15~40	0.01~1	SHV/TP	-	194/0
Thonon and Bontemps [30]	BPHE	-	R601, R600, R290	8.08/10/45°/-	300/300	26.9~70.3	1.5~18	2~18.5	0~1	SV/SL	-	52/0
Zhang et al. [18]	BPHE	7/8	R134a, R1234ze(E), R245fa, R1233zd(E)	3.4/4/65°/7	278/76	29.7~71.0	2.9~16.3	16~90	0~1	SHV/SCL	4.0~57.4	208/208
Soontarapiromsook et al. [51]	GPHE[f]	1/1	R134a	-/5/65°/-	360/100	40~50	10.2~13.2	61~89	0.1~0.8	TP/TP	5~15	96/96
Shon et al. [22]	BPHE	-	R1233zd(E)	3.32/3.88/60°/7.5	234/117	38.6~51.5	2~3	13.0~23.8	0.2~0.9	TP/TP	2.5~4.5	122/122
Overall range			HFCs, hydrocarbon, HFOs, CO_2	3.23~8.08/4~10/ 25.7°~70°/4.9~12	234~1092/ 72~486	-34.4 to 72.1	1.0~24.2	2~150	0~1		2.5~66.5	2376/1590

[a] Underlined data are obtained by calculation.
[b] SHV: Superheated vapor; SCL: Subcooled liquid; TP: Two-phase; SV: Saturated vapor; SL: Saturated liquid.
[c] N_{HT}: Number of heat transfer data; N_{PD}: Number of frictional pressure drop data.
[d] Number at condensation side/Number at cold water side.
[e] These cold water channels are curved tubes.
[f] These test sections are composed of three kind of plates with different surface roughness.

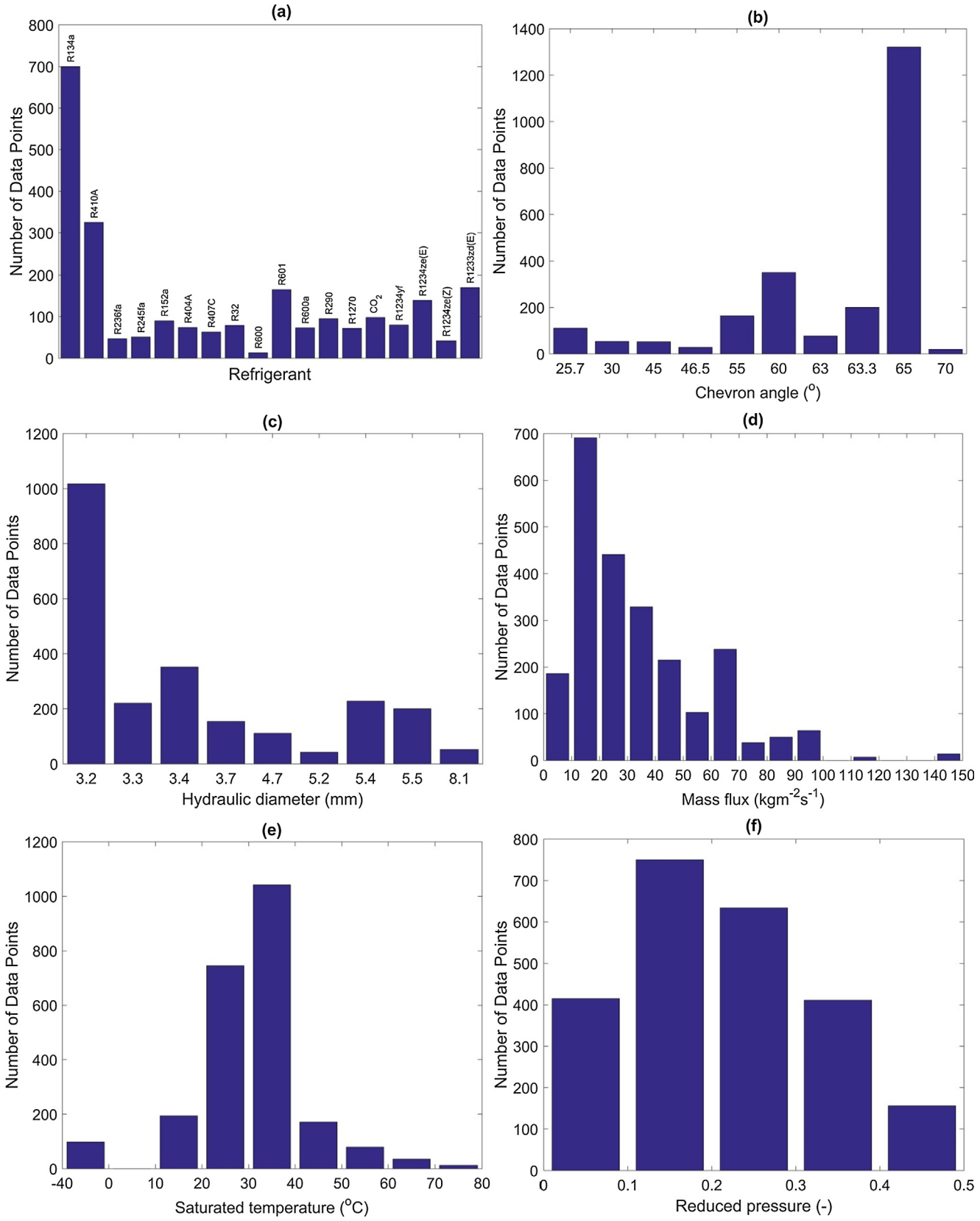

Fig. 1. Composition of the heat transfer database divided by (a) Refrigerants, (b) Chevron angles, (c) Hydraulic diameters, (d) Mass fluxes, (e) Saturated temperatures, (f) Reduced pressures.

4.1. Nusselt correlation

The classical Nusselt correlation shown in Eq. (19) was originally proposed for laminar film condensation on a vertical plate with saturated vapor [47]. Longo et al. [48] adopted Eq. (20) for saturated condensation in the gravity-controlled regime within PHEs. ϕ is the surface enlargement factor of the plates, and is the ratio of the actual heat transfer area to the projected area. Moreover, Webb [49] and Longo et al. [48] extended the application to superheated vapor by adding the de-superheating specific enthalpy change to the latent heat, as indicated in Eq. (21). The calculation agrees well with experimental data.

$$Nu_{gc} = 0.943\left[\frac{g\rho_L(\rho_L-\rho_G)L_p^3\Delta h_{LG}}{\mu_L\lambda_L\Delta T}\right]^{0.25} \tag{19}$$

$$Nu_{gc} = 0.943\phi\left[\frac{g\rho_L(\rho_L-\rho_G)L_p^3\Delta h_{LG}}{\mu_L\lambda_L\Delta T}\right]^{0.25} \tag{20}$$

$$\Delta h_{\sup} = \Delta h_{LG} + c_{p,G}(T_{\sup} - T_{sat}) \tag{21}$$

4.2. Akers correlation

Akers et al. [7] presented heat transfer correlations of convective condensation for horizontal tubes by using Re_{eq}, which is shown in Eq. (22). In Eq. (23), Longo et al. [48] calculated the HTCs of saturated vapor based on projected heat transfer areas, and ϕ is included. Yan et al. [20] chose different parameters as shown in Eq. (24). Zhang et al. [18] considered the influence of heat flux by including Bo in Eq. (25). Shon et al. [22] proposed Eq. (26) for R1233zd(E).

$$Nu_{cc} = \frac{\alpha_{cc}d_h}{\lambda_L} = aRe_{eq}^m Pr_L^n \tag{22}$$

$$Nu_{cc} = \frac{\alpha_{cc}d_h}{\lambda_L} = 1.875\phi Re_{eq}^{0.445} Pr_L^{0.333} \tag{23}$$

$$Nu_{cc} = \frac{\alpha_{cc}d_h}{\lambda_L} = 4.118 Re_{eq}^{0.4} Pr_L^{0.333} \tag{24}$$

$$Nu_{cc} = \frac{\alpha_{cc}d_h}{\lambda_L} = 4.3375 Re_{eq}^{0.5383} Pr_L^{0.333} Bo^{-0.3872} \tag{25}$$

$$Nu_{cc} = \frac{\alpha_{cc}d_h}{\lambda_L} = 2.337 Re_{eq}^{1.024} Re_{LO}^{-0.294} Pr_L^{0.333} Bo_{eq}^{0.361} \tag{26}$$

Han et al. [50] added geometric parameters to the basic Akers correlation as shown in Eq. (27), where Λ_{wave} is the corrugation wave length and β is the chevron angle in the unit of radian. In Eq. (28), Soontarapiromsook et al. [51] considered the surface roughness of the plates, whose influence is relatively small compared with chevron angles.

$$Nu_{cc} = \frac{\alpha_{cc}d_h}{\lambda_L} = \left(11.22\left(\frac{\Lambda_{wave}}{d_h}\right)^{-2.83}\beta^{-4.5}\right) Re_{eq}^{\left(0.35\left(\frac{\Lambda_{wave}}{d_h}\right)^{0.23}\beta^{1.48}\right)} Pr_L^{0.333} \tag{27}$$

$$Nu_{cc} = \frac{\alpha_{cc}d_h}{\lambda_L} = 5.095\times10^{-6} Re_{eq}^{0.566} Pr_L^{9.753}\left(\frac{\delta}{d_h}\right)^{0.121} \tag{28}$$

The correlation of Würfel and Ostrowski [52] also involves geometry as shown in Eq. (29), and is based on projected heat transfer areas. This Reynolds number is calculated in Eq. (30). Both Nu_{cc} and Re_h depend on the chevron angles of neighbouring plates, which are listed in Table. 2. The vapor quality in Eq. (30) is the averaged value and is 0.5 for complete condensation.

Table 2
Constants in Eqs. (29) and (30), depending on the plate combination.

Plates	a	m	k
30°/30°	0.325	0.62	0.4
30°/60°	3.2	0.46	0.3
60°/60°	3.77	0.43	0.14

$$Nu_{cc} = \frac{\alpha_{cc}d_h}{\lambda_L} = aRe_h^m Pr_L^{0.333} \tag{29}$$

$$Re_h = \frac{G[(1-x_{av}) + x_{av}(\rho_L/\rho_G)^k]d_h}{\mu_L} \tag{30}$$

4.3. Webb correlation

In Eq. (31), Webb [49] proposed a theoretical model for superheated condensation inside tubes, and applied this model to the inside of enhanced tubes and outside of a bundle of tubes. The driving temperature difference is between saturated temperature and wall temperature. Both latent heat and sensible heat contribute to heat transfer. α_{sat} is the condensation HTC of saturated vapor, α_G is the single-phase HTC between superheated vapor and two-phase interface. $c_{p,G}\dot{q}_{LG}/\Delta h_{LG}$ accounts for the movement of the condensing vapor to the interface, which enhances single-phase heat transfer, where $\dot{q}_{LG}$ is the local heat flux due to phase change only. The temperature ratio term approaches zero as the superheating vanishes. Longo et al. [48] extended this model to PHEs.

$$\alpha_{\sup} = \alpha_{sat} + \frac{T_{\sup} - T_{sat}}{T_{sat} - T_{wall}}\left(\alpha_G + \frac{c_{p,G}\dot{q}_{LG}}{\Delta h_{LG}}\right) \tag{31}$$

4.4. Shah correlation

Shah [53] presented a correlation for condensation in horizontal, vertical, and inclined tubes by modifying the liquid only HTC, which is shown in Eqs. (32) and (33). Liquid only HTC, α_{LO}, assumes all the fluid is liquid, and in fact single-phase HTC applies. Vapor quality and reduced pressure were included. This correlation was verified by extensive experimental data, and was widely adopted to PHEs. Since the geometric structures of both condensation side and cooling water side are the same, the same correlation is expected to apply to α_{LO} and the HTC of cooling water. Kuo et al. [16] presented the single-phase heat transfer correlations of both refrigerant and cooling water, which are almost the same [20].

$$\alpha_{cc} = \alpha_{LO}\left((1-x)^{0.8} + \frac{3.8x^{0.76}(1-x)^{0.04}}{(P_{sat}/P_{cr})^{0.38}}\right) \tag{32}$$

$$\alpha_{LO} = 0.023 Re_{LO}^{0.8} Pr_L^{0.4}\frac{\lambda_L}{d_h} \tag{33}$$

Shi et al. [21] determined the parameters in Eq. (34) by minimizing the prediction errors, but α_{LO} is not given. Since this correlation is derived from the experimental data of local measurement, it is considered to predict the local heat transfer performance. Additionally, Eqs. (35) and (36) from Thonon and Bontemps [30] are based on gravity-controlled condensation, and include the enhancement influence of corrugated structures. These correlations calculate the HTCs of projected heat transfer areas. Kuo et al. [16] proposed HTC in Eqs. (37) and (38), which is a function of Co_2 in Eq. (3), Fr_L in Eq. (13) and Bo in Eq. (16).

$$\alpha_{cc} = \alpha_{LO}\left((1-x)^{0.8} + \frac{3.00388x^{1.296}}{(1-x)^{0.496}(P_{sat}/P_{cr})^{0.648}}\right) \tag{34}$$

$$\alpha_{cc} = 1564 Re_{eq}^{-0.76}\alpha_{LO} \tag{35}$$

$$\alpha_{LO} = 0.347 Re_{LO}^{0.653} Pr_L^{0.33}\frac{\lambda_L}{d_h} \tag{36}$$

$$\alpha_{cc} = \alpha_{LO}\left(0.25 Co_2^{-0.45} Fr_L^{0.25} + 75 Bo^{0.75}\right) \tag{37}$$

$$\alpha_{LO} = 0.2092 Re_{LO}^{0.78} Pr_L^{0.333}\left(\frac{\mu_{av}}{\mu_{wall}}\right)^{0.14}\frac{\lambda_L}{d_h} \tag{38}$$

Palmer et al. [19] developed correlations for low mass flux and heat flux. They tested a heat pump system using several refrigerants, which contained two kinds of lubricants. The different trends of the experimental data indicate the influence of lubricants, leading to two correlations. R22, R290 and R290/R600a were lubricated with mineral oil, and the correlation is presented in Eqs. (39)–(41). α_L is liquid HTC and assumes that the liquid phase flows alone, ϕ_L is the two-phase friction multiplier; Lockhart-Martinelli parameter, X_{tt}, is calculated in Eq. (1); Ga is calculated in Eq. (14). R32/R152a was lubricated with polyol ester oil and was calculated by Eq. (42).

$$\alpha_{cc} = \alpha_L^{0.387}\phi_L^{0.0824} Ga^{0.346}\left(\frac{P_{sat}}{P_{cr}}\right)^{1.5}\left[-\lg\left(\frac{P_{sat}}{P_{cr}}\right)\right]^{1.5}\left(\frac{\lambda_L}{d_h}\right)^{0.613} \tag{39}$$

$$\alpha_L = 0.16 Re_L^{0.89} Pr_L^{0.3}\frac{\lambda_L}{d_h} \tag{40}$$

$$\phi_L = \left(1 + \frac{12}{X_{tt}} + \frac{1}{X_{tt}^2}\right)^{0.5} \tag{41}$$

$$\alpha_{cc} = \alpha_L^{0.298} Ga^{0.346}\left(\frac{P_{sat}}{P_{cr}}\right)^{1.5}\left[-\lg\left(\frac{P_{sat}}{P_{cr}}\right)\right]^{1.5}\left(\frac{\lambda_L}{d_h}\right)^{0.702} \tag{42}$$

4.5. Mancin correlation

Mancin et al. [34] proposed to combine gravity-controlled condensation and convective condensation in Eq. (43). Nusselt correlation in Eq. (19) was used for gravity-controlled condensation. The correlation from Cavallini et al. [54] was chosen for convective condensation in Eq. (44), which also includes α_{LO}.

$$\alpha_c = \left(\alpha_{gc}^2 + \alpha_{cc}^2\right)^{0.5} \tag{43}$$

$$\alpha_{cc} = \alpha_{LO}\left(1 + 1.128x^{0.817}\left(\frac{\rho_L}{\rho_G}\right)^{0.3685}\left(\frac{\mu_L}{\mu_G}\right)^{0.2363}\left(1 - \frac{\mu_G}{\mu_L}\right)^{2.144} Pr_L^{-0.1}\right) \tag{44}$$

Mancin et al. [36] improved this correlation by considering the transition between gravity-controlled condensation (temperature driving force dependent regime) and convective condensation (temperature driving force independent regime) proposed by Cavallini et al. [54]. The transition is determined by non-dimensional gas velocity, j_G and the following equations.

$$\begin{cases} j_G \le j_{G\_low}, & \text{gravity} - \text{controlled condensation} \\ j_{G\_low} < j_G < j_{G\_high}, & \text{transition regime} \\ j_G \ge j_{G\_high}, & \text{convective condensation} \end{cases} \tag{45}$$

where

$$j_G = \frac{xG}{[g d_h \rho_G(\rho_L - \rho_G)]^{0.5}} \tag{46}$$

and

$$j_{G\_low} = 0.89 - 0.93 e^{-0.087\left[\left(\frac{1}{x}-1\right)^{0.8}\left(\frac{P_{sat}}{P_{cr}}\right)^{0.4}\right]^{-1.17}} \tag{47}$$

$$j_{G\_high} = \left[\left(\frac{7.5}{4.3\left(\left(\frac{\mu_L}{\mu_G}\right)^{0.1}\left(\frac{\rho_G}{\rho_L}\right)^{0.5}\left(\frac{1-x}{x}\right)^{0.9}\right)^{1.11} + 1}\right)^{-3} + 2.6^{-3}\right]^{-0.333} \tag{48}$$

Eq. (49) gives the HTC of gravity-controlled condensation, while Eq. (44) calculates convective condensation. Eq. (50) is applied in the transition regime.

$$Nu_{gc} = 1.1316\left[\frac{g\rho_L(\rho_L - \rho_G)L_p^3\Delta h_{LG}}{\mu_L\lambda_L\Delta T}\right]^{0.25} \tag{49}$$

$$\alpha_c = \alpha_{gc} + (\alpha_{cc} - \alpha_{gc})\frac{j_G - j_{G\_low}}{j_{G\_high} - j_{G\_low}} \tag{50}$$

4.6. Wang correlation

In Eq. (51), Wang and Zhao [23] considered the subcooling of condensate. The density ratio indicates the influence of reduced pressure. Re_L is defined in Eq. (8) with the vapor quality of the PHE outlet, which shows the feature of partial condensation. Ja is calculated in Eq. (18). Jokar et al. [17] added more property parameters in Eq. (52).

$$Nu_{cc} = \frac{\alpha_{cc} d_h}{\lambda_L} = 0.00115\left(\frac{Re_L}{Ja}\right)^{0.983} Pr_L^{0.333}\left(\frac{\rho_L}{\rho_G}\right)^{0.248} \tag{51}$$

$$Nu_{cc} = \frac{\alpha_{cc} d_h}{\lambda_L} = 3.371 Re_L^{0.55} Pr_L^{0.3} Ja^{-1.05}\left(\frac{G^2}{\rho_L^2 c_{p,L}(T_{sat} - T_{wall})}\right)^{0.25} \times \left(\frac{\rho_L\sigma}{\mu_L G}\right)^{0.05}\left(\frac{\rho_L}{\rho_L - \rho_G}\right)^2 \tag{52}$$

Hayes et al. [24] presented Eq. (53) and Table. 3, which are derived from the complete condensation of CO_2 by excluding the single-phase areas of de-superheating and subcooling. The tested PHEs had three combinations of chevron angles.

$$Nu_{cc} = \frac{\alpha_{cc} d_h}{\lambda_L} = C_1 Re_{LO}^{C_2} Pr_L^{C_3} Ja^{C_4}\left(\frac{G^2}{\rho_L^2 c_{p,L}(T_{sat} - T_{wall})}\right)^{C_5}\left(\frac{\rho_L\sigma}{\mu_L G}\right)^{C_6}\left(\frac{\rho_L}{\rho_L - \rho_G}\right)^{C_7} \tag{53}$$

4.7. Winkelmann correlation

Winkelmann [15] claimed that vapor quality is more influential than mass flux. According to Eq. (54), the Convection number, Co, as shown in Eq. (2), is more relevant than Re_{eq}.

$$Nu_{cc} = \frac{\alpha_{cc} d_h}{\lambda_L} = 94 Co^{-0.46} Pr_L^{0.333} \qquad 0.07 < Co < 0.28 \tag{54}$$

4.8. Correlation for mixtures

In order to predict mixture condensation, Thonon and Bontemps [30] referred to the correlation of Silver [55] and Bell and Ghaly [56] in Eq. (55). Molecular diffusion in the vapor phase

Table 3
Constants and application range of Eq. (53), depending on the plate combinations.

Plates	C_1	C_2	C_3	C_4	C_5	C_6	C_7	Re_{LO}
30°/30°	0.37	0.706	0.35	−0.91	0.16	0.032	1.18	67–1276
30°/63°	0.16	0.727	0.35	−0.90	0.17	0.147	1.00	164–1233
63°/63°	0.11	0.771	0.35	−0.92	0.12	0.0105	2.00	129–1156

induces mass transfer resistance, and deteriorates the heat transfer. The mass transfer resistance is assumed to be proportional to the heat transfer resistance of the vapor, α_G^{-1}, and derivative of temperature with enthalpy, dT/dh.

$$\alpha_{c,mix} = \left(\alpha_{c,pure}^{-1} + x c_{p,G} \frac{dT}{dh} \alpha_G^{-1}\right)^{-1} \tag{55}$$

5. Assessment of heat transfer correlations

Generally, the basic forms of heat transfer correlations only include the dominant parameters. In order to improve the accuracy in certain operating conditions, the modified forms change the indexes and multipliers, or involve the parameters of fluid property and geometry. But the modifications are not certainly applicable beyond the tested range. In this section, eight correlations are compared with the database introduced in Section 3, and are assessed in wider ranges. These correlations are representative for the different basic forms. The correlations of Longo et al. [48] and Thonon and Bontemps [30] are derived from projected heat transfer areas, and are converted to the HTCs of actual heat transfer areas during the comparison.

Several assumptions are made to supplement the missing information:

- For the experimental data of superheated inlet and subcooled outlet, some researchers subtracted the single-phase areas for de-superheating and subcooling [24,37,26,15,27,28,21], while others assumed no single-phase region when the superheating degree or subcooling degree is small [31–36]. In these cases, the vapor qualities are taken as 1 or 0. The averaged vapor quality of 0.5 and saturated temperature are inputted to calculate the HTC. This assumption can be further validated with new researches which include superheating and subcooling.
- The surface enlargement factor, ϕ, is calculated from channel gap and corrugation wavelength. The hydraulic diameter, d_h, is the ratio of the equivalent diameter, d_e to ϕ [57,4].
- The heat flux varies with mass flux, and is used to calculate *Bo*. When not specified, the heat flux is determined by the enthalpy change and heat transfer area.
- The temperature difference between the condensate and wall is reported in Mancin et al. [34–36] and Hayes et al. [24]. It is calculated from the heat flux and experimental HTC when not specified. This temperature difference is involved in the HTCs for gravity-controlled condensation and Jakob number, *Ja*.

In Fig. 2(a), the correlation of Longo et al. [48] predicts 93.0% of the experimental data within ±50%, which is the best prediction among the selected correlations. Large data, which correspond to large mass fluxes and high vapor qualities, are slightly under-predicted. The possible reason is that this correlation is derived from the experimental data of complete condensation, and the mass fluxes are less than 45 $kg{\cdot}m^{-2}{\cdot}s^{-1}$. The experimental data of CO_2 [24] are over-predicted since the fluid properties are significantly different from other refrigerants. The thermal conductivity of liquid CO_2 is large, and the reduced pressure is high during condensation. This over-prediction is more significant for small HTCs.

In Fig. 2(b), the prediction of Yan et al. [20] is similar to Longo et al. [48], but low HTCs, which correspond to small mass fluxes, are over-predicted. This correlation predicts more than half of the experimental data within ±50%. It has been developed from partial condensation in the range of 60–120 $kg{\cdot}m^{-2}{\cdot}s^{-1}$ and for the averaged vapor qualities of 0.1–0.9.

In Fig. 2(c), the prediction of Han et al. [50] is lower than a large portion of the experimental data, and shows sensitivity to geometric parameters. As shown in Table 1, the experimental data of Han et al. [50] were obtained from three geometries, where d_h and Λ_{wave} are smaller than for most of the other papers. This correlation seems to be only applicable to the tested geometric parameters.

In Fig. 2(d), the correlation of Kuo et al. [16] slightly under-predicts the experimental data. 88.4% of the experimental data are predicted within ±50%, which is the second best. This correlation involves the influence of heat flux by using *Bo*, and the heat flux is in the range of 10000–20000 $W\,m^{-2}$. The under-prediction of Thonon and Bontemps [30] and Han et al. [50] is noticeable as these experimental data had smaller heat fluxes.

In Fig. 2(e), the correlation of Thonon and Bontemps [30] predicts their own data accurately, but the predicted values decrease with the experimental data from other researchers. It is derived from the experimental data of small mass fluxes (around 2–20 $kg{\cdot}m^{-2}{\cdot}s^{-1}$). According to this correlation, the HTCs decrease with increasing mass fluxes for gravity-controlled condensation, but this sensitivity is over-estimated. It is not suitable for convective condensation, especially at large mass fluxes.

In Fig. 2(f), the correlation of Palmer et al. [19] over-predicts most of the experimental data. The working fluid of this correlation is the mixture of several refrigerants and oil. Moreover, it is developed for small mass fluxes.

In Fig. 2(g), the correlation of Mancin et al. [34] combines gravity-controlled condensation and convective condensation using an asymptotic power-law. This correlation was recommended by Sarraf et al. [26]. Sarraf et al. [26] used an infrared camera to measure the end plates temperature of both working fluid side and cold water side. The temperature difference between the plate and fluid is assumed to be negligible, and the plate temperature represents the fluid. These local HTCs span a large range and cannot be predicted by other correlations. Sarraf et al. [26] argued that the local HTCs based on infrared measurement are higher than the overall HTCs. Constant heat flux is assumed to determine the overall HTCs, but this assumption can hardly be reasonable.

In Fig. 2(h), the correlation of Hayes et al. [24] is the only one proposed for CO_2, but over-predicts most of the other refrigerants. This correlation excludes the areas of de-superheating and subcooling regions during data reduction, without considering vapor qualities. It is developed using dimensional analysis. The applicability seems to be limited to the complete condensation of CO_2.

The correlation of Longo et al. [48] is derived from the complete condensation of several refrigerants as shown in Table 1. The mass fluxes are 5–45 $kg{\cdot}m^{-2}{\cdot}s^{-1}$. This correlation can be expanded to the ranges described in Table 1, but is less suitable for $CO_2{\cdot}NH_3$ is not

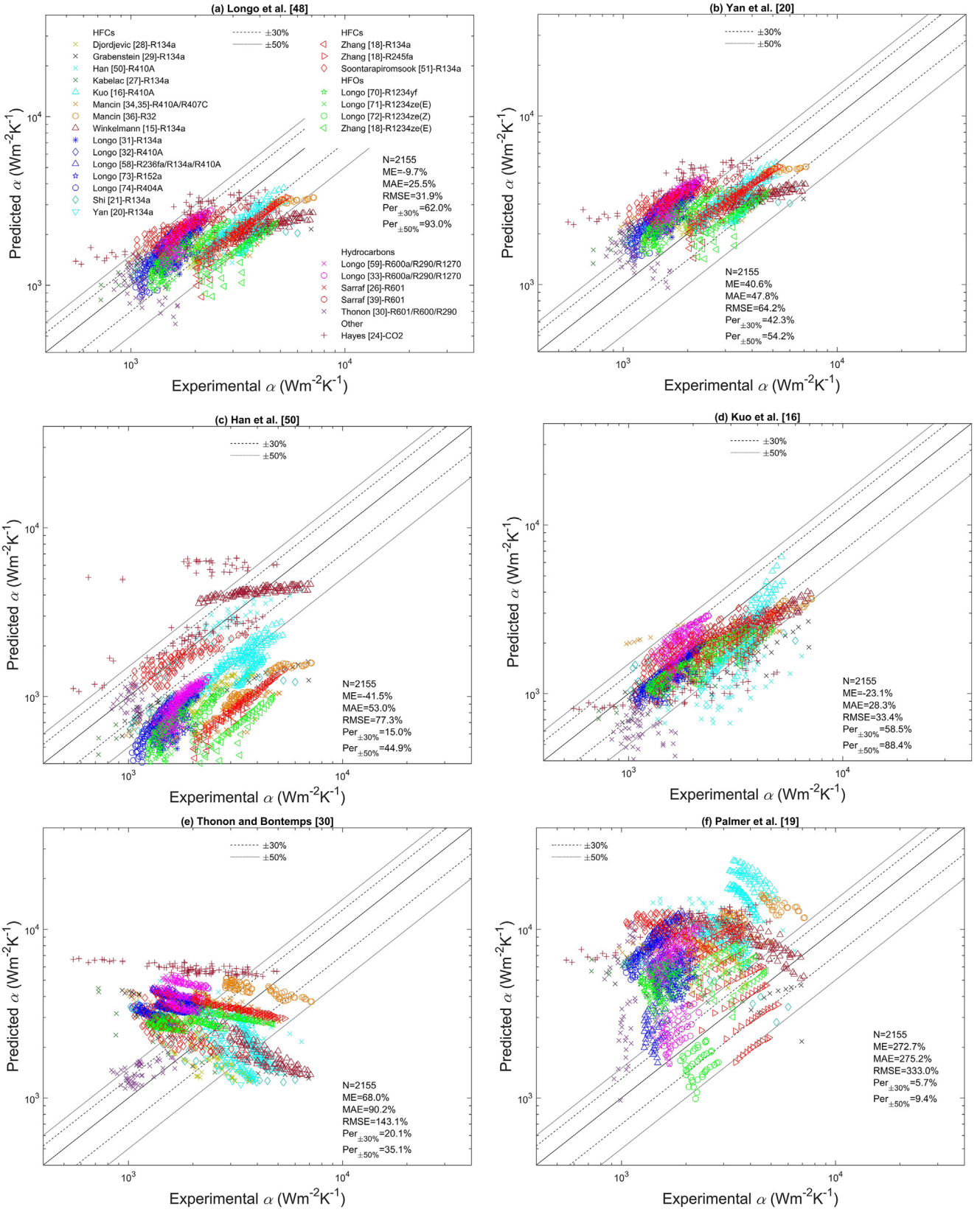

Fig. 2. Comparison of heat transfer correlations with experimental data: (a) Longo et al. [48], (b) Yan et al. [20], (c) Han et al. [50], (d) Kuo et al. [16], (e) Thonon and Bontemps [30], (f) Palmer et al. [19], (g) Mancin et al. [34], (h) Hayes et al. [24]. Number of experimental data (N); Mean error (ME): $\frac{1}{n}\sum_1^n \frac{\alpha_{pre}-\alpha_{exp}}{\alpha_{exp}}$; Mean absolute error (MAE): $\frac{1}{n}\sum_1^n \left|\frac{\alpha_{pre}-\alpha_{exp}}{\alpha_{exp}}\right|$; Root mean squared error (RMSE): $\sqrt{\frac{1}{n}\sum_1^n \left(\frac{\alpha_{pre}-\alpha_{exp}}{\alpha_{exp}}\right)^2}$; $Per_{\pm 30\%}$: Percentage of experimental data within ±30%; $Per_{\pm 50\%}$: Percentage of experimental data within ±50%.

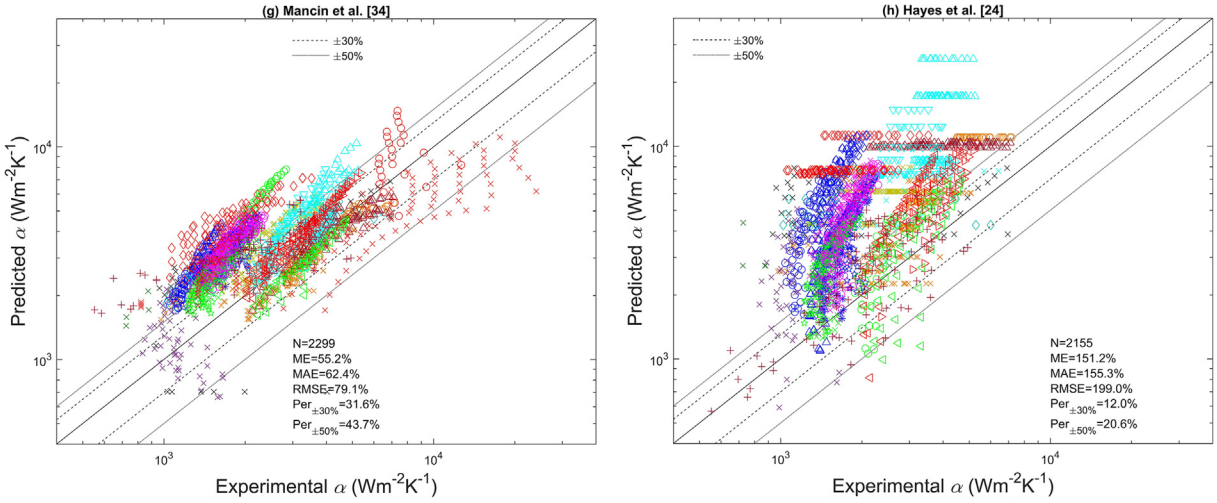

Fig. 2 (*continued*)

included in the database and requires further investigation. During the condensation in PHEs, gravity-controlled condensation takes place at small mass fluxes and low vapor qualities [58,59,34,35,30,26]. Eq. (23) is originally developed for convective condensation, and predicts the HTCs of gravity-controlled condensation within ±50%. The authors argued that gravity-controlled condensation is transited to convective condensation at Re_{eq} of 1600.

Condensation mechanisms are affected by vapor qualities, whose influence is remarkable during partial condensation. The condensation mechanisms are determined by the two-phase flow distribution and interaction at the interface. The correlation of Longo et al. [48] involves Re_{eq}, and assumes homogeneous two-phase flow. The equivalent fluid properties are considered as a combination of liquid and vapor [7]. The correlation of Kuo et al. [16] assumes separated flow, and also shows satisfactory prediction. This correlation calculates the liquid only HTCs, and considers the heat transfer enhancement contributed by vapor flow and heat flux [14,53]. The knowledge of flow patterns helps to develop a mechanistic model for condensation within PHEs [60,61,54].

6. Frictional pressure drop correlations

Tao et al. [4] summarized the influencing factors of frictional pressure drop. The contributing factors of heat transfer generally increase frictional pressure drop. Despite the condensation mechanisms, frictional pressure drop increases with mass flux and vapor quality monotonically. Additionally, plate geometry, condensation pressure, superheating and heat flux are considered as influential. This section presents frictional pressure drop correlations. Amalfi et al. [8] suggested to classify the two-phase frictional pressure drop correlations into three types. Two-phase Fanning friction factors assume homogeneous flow, while Lockhart-Martinelli's model is based on separated flow. Kinetic energy model is originally proposed by modifying the homogeneous void fraction model. Lockhart-Martinelli model and Kinetic energy model were first developed for adiabatic flow and later extended to condensation.

6.1. Two-phase Fanning friction factor

Two-phase Fanning friction factors assume homogeneous flow, and the two-phase flow is regarded as single fluid flow. The frictional pressure drop is calculated similarly to single-phase in Eq. (56).

$$\Delta P_{TP} = 2 f_{TP} \frac{G^2}{\rho_{av}} \frac{L_p}{d_h} \tag{56}$$

Kuo et al. [16] presented a correlation including Re_{eq} and Bo in Eq. (57). The correlation of Yan et al. [20] in Eq. (58) is similar, but under-predicts the experimental database significantly. The predictions of Eq. (59) from Shi et al. [21] are also lower than the experimental data. In Eq. (60), Zhang et al. [18] used We_{homo} to involve surface tension. Shon et al. [22] proposed a correlation as given in Eq. (61).

$$f_{TP} = 21500 Re_{eq}^{-1.14} Bo^{-0.085} \tag{57}$$

$$f_{TP} = 94.75 Re_{eq}^{-0.0467} Re_{LO}^{-0.4} Bo^{0.5} \left(\frac{P_{sat}}{P_{cr}}\right)^{0.8} \tag{58}$$

$$f_{TP} = 350188 Re_{eq}^{-2.19} Bo_{eq}^{-0.23} \tag{59}$$

$$f_{TP} = 0.0146 Re_{eq}^{0.9814} We_{eq}^{-1.0064} \tag{60}$$

$$f_{TP} = 1261.067 Re_{eq}^{-0.411} Re_{LO}^{-0.57} \tag{61}$$

Han et al. [50] considered geometric parameters in Eq. (62). Accordingly, frictional pressure drop increases with chevron angles dramatically. Soontarapiromsook et al. [51] investigated the surface roughness of the plates and proposed Eq. (63). In Eq. (64), Jokar et al. [17] used the modified liquid only Reynolds number, Re_{mod}, calculated from the averaged dynamic viscosity in Eq. (10).

$$f_{TP} = \left(3521.1 \left(\frac{\Lambda_{wave}}{d_h}\right)^{4.17} \beta^{-7.75}\right) Re_{eq}^{\left(-1.024 \left(\frac{\Lambda_{wave}}{d_h}\right)^{0.0925} \beta^{-1.3}\right)} \tag{62}$$

$$f_{TP} = 2671.743 Re_{eq}^{-0.818} \left(\frac{\delta}{d_h}\right)^{0.065} \tag{63}$$

$$f_{TP} = 2.139 \times 10^7 Re_{mod}^{-1.6} \qquad 960 < Re_{mod} < 4160 \tag{64}$$

Hayes et al. [37] tested CO_2 condensation in the same PHEs as the experiments leading to Eq. (53) and Table. 3, and proposed Eq. (65) and Table. 4. This correlation depends on the chevron angles of the PHEs.

$$f_{TP} = C_1 Re_{LO}^{C_2} \tag{65}$$

Table 4
Constants of Eq. (65), depending on the plate combinations.

Plates	C_1	C_2
30°/30°	1837.4	−0.817
30°/63°	10.65	0
63°/63°	1221.3	−0.815

Amalfi et al. [8–9] developed a comprehensive database of two-phase frictional pressure drop under evaporative and adiabatic conditions, and proposed Eq. (66). This correlation predicts their database well. β/β_{max} is the ratio of chevron angle, where β_{max} is the maximum chevron angle and is 70°.

$$f_{TP} = 15.698\left(2.125\left(\frac{\beta}{\beta_{max}}\right)^{9.993} + 0.955\right) We_{homo}^{-0.475} Bd^{0.255} \left(\frac{\rho_L}{\rho_G}\right)^{-0.571} \tag{66}$$

6.2. Lockhart-Martinelli model

Lockhart-Martinelli model [12] was originally proposed in a graphical form, and was further developed by Chisholm [62] into correlations in Eqs. (67)–(69). This model is derived from the separated, adiabatic flow of air and liquids in tubes. C is determined by the flow regime combinations of liquid and vapor (laminar or turbulent). X is the Lockhart-Martinelli parameter; ϕ_L is the two-phase friction multiplier. In Eqs. (70) and (71), the liquid frictional pressure drop, ΔP_L, presumes the liquid flows alone; the vapor frictional pressure drop, ΔP_G, assumes the vapor flows alone; ΔP_{TP} is the two-phase frictional pressure drop.

$$\phi_L^2 = 1 + \frac{C}{X} + \frac{1}{X^2} \tag{67}$$

$$X^2 = \frac{\Delta P_L}{\Delta P_G} \tag{68}$$

$$\phi_L^2 = \frac{\Delta P_{TP}}{\Delta P_L} \tag{69}$$

$$\Delta P_L = 2f_L \frac{G_L^2}{\rho_L}\frac{L_p}{d_h} = 2f_L \frac{G^2(1-x)^2}{\rho_L}\frac{L_p}{d_h} \tag{70}$$

$$\Delta P_G = 2f_G \frac{G_G^2}{\rho_G}\frac{L_p}{d_h} = 2f_G \frac{G^2 x^2}{\rho_G}\frac{L_p}{d_h} \tag{71}$$

In Eq. (72), Winkelmann [15] predicted his experimental data of adiabatic air-water and condensing R134a within PHEs. The single-phase Fanning friction factors of liquid and vapor are calculated in Eq. (73), where the Reynolds number is Re_L in Eq. (8) and Re_G in Eq. (9).

$$\phi_L^2 = 1 + \frac{6}{X} + \frac{1}{X^2} \qquad 0.01 \le X \le 1 \tag{72}$$

$$f = \begin{cases} 0.3 + 53\mathrm{Re}^{-1}, & 10 < \mathrm{Re} < 1700 \\ \mathrm{Re}^{-0.135}, & 1700 < \mathrm{Re} < 50000 \end{cases} \tag{73}$$

In Eq. (74), Nilpueng and Wongwises [63] modified the original model to predict their experimental data of upward and downward flow. The single-phase Fanning friction factor is calculated in Eq. (75).

$$\phi_L^2 = 1.339 + \frac{4.492}{X} \tag{74}$$

$$f = 4.929\mathrm{Re}^{-0.22} \tag{75}$$

Wang and Zhao [23] extended this model to steam condensation in a PHE, and proposed a graphical relation between X and ϕ_L.

Würfel and Ostrowski [52] proposed Eq. (76) for the condensation of water and n-heptane. F depends on the chevron angles of plates in Table. 5. X_{tt} is calculated in Eq. (1) for turbulent-turbulent flow.

$$\phi_L^2 = \frac{F}{X_{tt}^2} \tag{76}$$

6.3. Kinetic energy model

In Eqs. (77) and (78), Jassim et al. [64] developed a kinetic energy model for adiabatic two-phase flow within PHEs, which was in vertical upward direction. KE/V is the kinetic energy per unit volume. The void fraction, ε, depends on the prevailing flow patterns. The homogeneous void fraction model over-predicts the kinetic energy, while the selected separated flow models under-predict the kinetic energy. Thus an effective void fraction was recommended by modifying the homogeneous model. The effective void fraction is between the values of homogeneous and separated models, and depends on the PHE structures. The authors concluded that inertial effects, rather than viscous effects, dominate the frictional pressure drop.

$$\Delta P_{TP} = \zeta \frac{KE}{V} = \zeta \frac{G^2}{2\rho_{av}} \tag{77}$$

$$\rho_{av} = (1-\varepsilon)\rho_L + \varepsilon\rho_G \tag{78}$$

Longo [58–59] adopted the kinetic energy model for condensation in a PHE, which was vertically downward. The flow is assumed to be homogeneous and is represented by the averaged two-phase density in Eq. (4). ζ is 2 for HFCs and 1.9 for hydrocarbons.

7. Assessment of frictional pressure drop correlations

This section compares six representative correlations with the experimental database collected in Section 3. ζ of the kinetic energy model depends on the PHE structures. Thus this model is not accessed. The majority of experiments have been carried out to obtain both heat transfer and frictional pressure drop data, and the operating conditions are the same. The assumptions for heat transfer data in Section 5 also apply to this section. The frictional pressure drop is compared in gradient form. Some experimental data have superheated inlet and subcooled outlet. Sarraf et al. [39] and Hayes et al. [37] excluded the single-phase areas and obtained the two-phase pressure drop, but the lengths of two-phase areas were not given. Djordjević et al. [28] and Shi et al. [21] tested the local frictional pressure drop without providing the test length. Thus these experimental data could not be included. Xiao and Hrnjak [40] suggested to predict frictional pressure drop of two-phase from the onset of condensation. When the superheating degree or subcooling degree is small and no single-phase region is assumed, the lengths of two-phase regions are the same as the PHE lengths [31–36].

Table 5
Constants in Eq. (76), depending on the plate combinations.

Plates	30°/30°	30°/60°	60°/60°
F	0.1	0.1	0.5

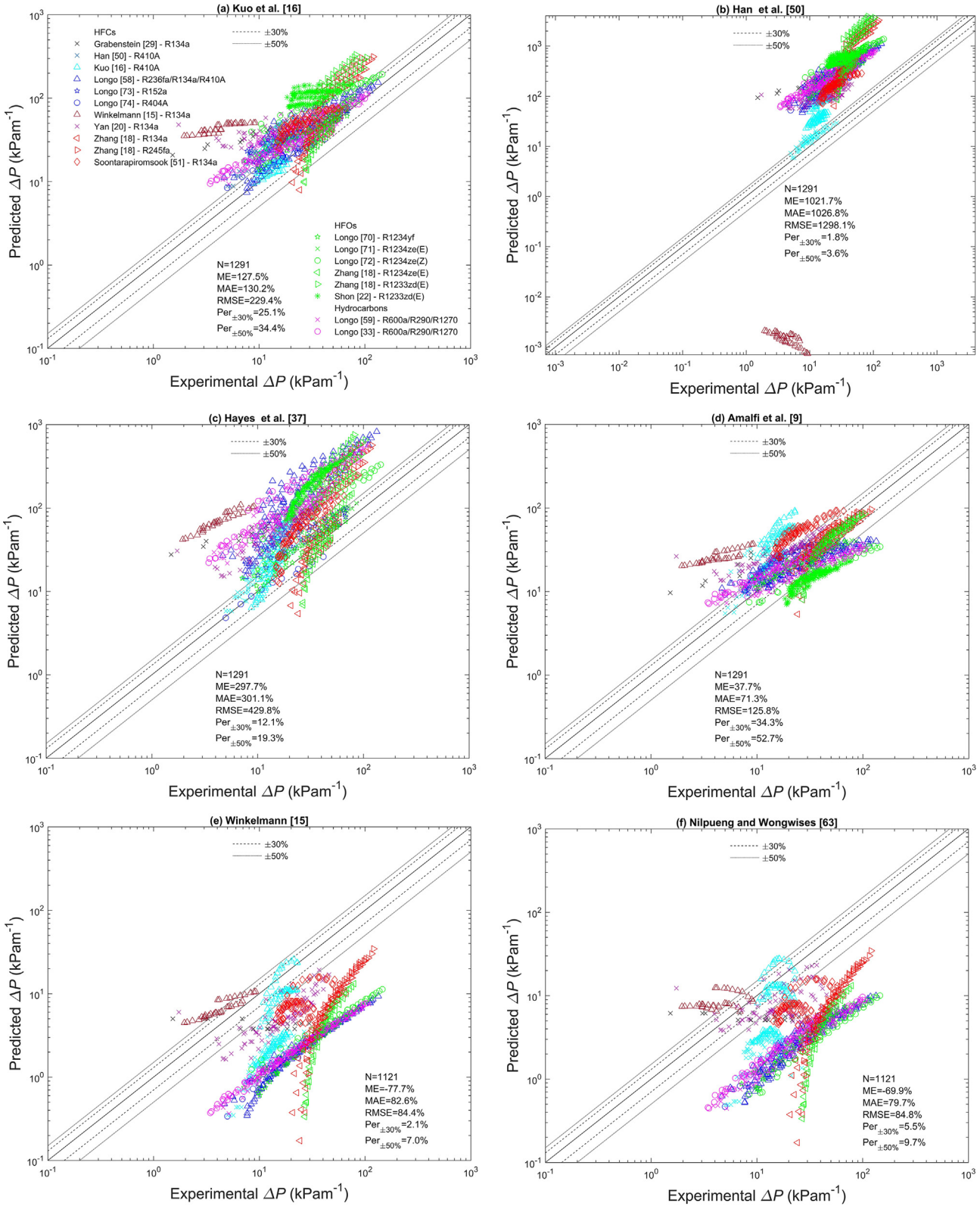

Fig. 3. Comparison of frictional pressure drop correlations with the experimental data: (a) Kuo et al. [16], (b) Han et al. [50], (c) Hayes et al. [37], (d) Amalfi et al. [9], (e) Winkelmann [15], (f) Nilpueng and Wongwises [63]. Number of experimental data (N); Mean error (ME): $\frac{1}{n}\sum_1^n \frac{\Delta P_{pre}-\Delta P_{exp}}{\Delta P_{exp}}$; Mean absolute error (MAE): $\frac{1}{n}\sum_1^n \frac{|\Delta P_{pre}-\Delta P_{exp}|}{\Delta P_{exp}}$; Root mean squared error (RMSE): $\sqrt{\frac{1}{n}\sum_1^n \left(\frac{\Delta P_{pre}-\Delta P_{exp}}{\Delta P_{exp}}\right)^2}$; $Per_{\pm 30\%}$: Percentage of experimental data within ±30%; $Per_{\pm 50\%}$: Percentage of experimental data within ±50%.

In Fig. 3(a), the prediction of Kuo et al. [16] is generally higher than the experimental data. The data are more scattered for small pressure drop, which corresponds to small mass fluxes.

In Fig. 3(b), the correlation of Han et al. [50] predicts their data well but is not applicable for other experiments. Eq. (62) is especially sensitive to chevron angles, which over-predicts the experi-

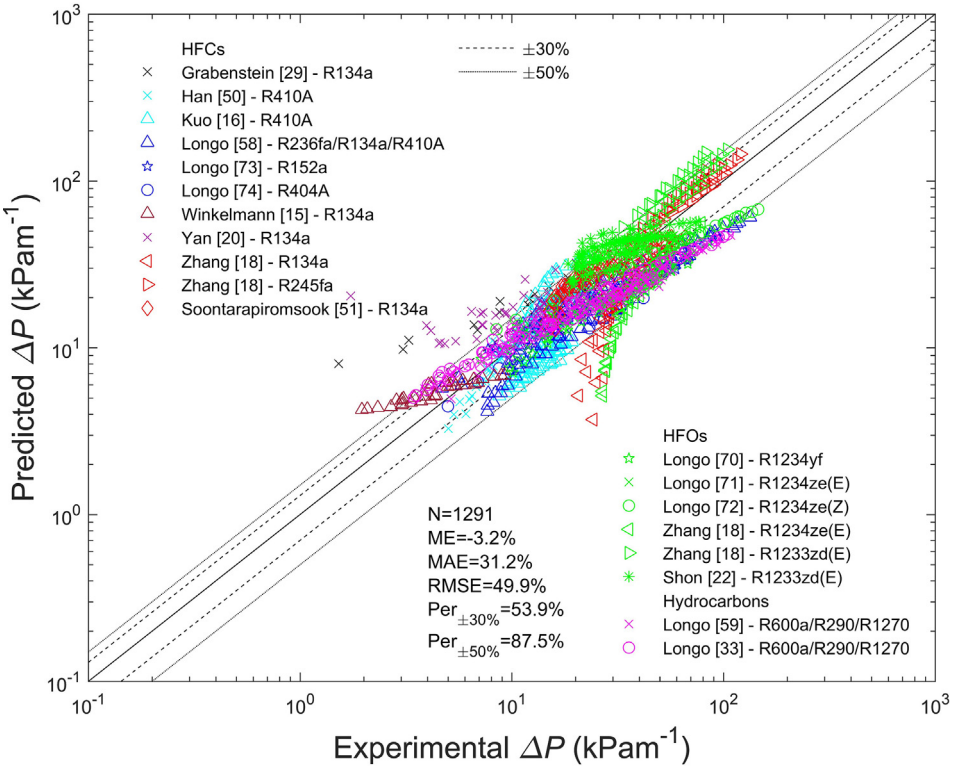

Fig. 4. Comparison of the new frictional pressure drop correlation, Eq. (80), with the experimental data.

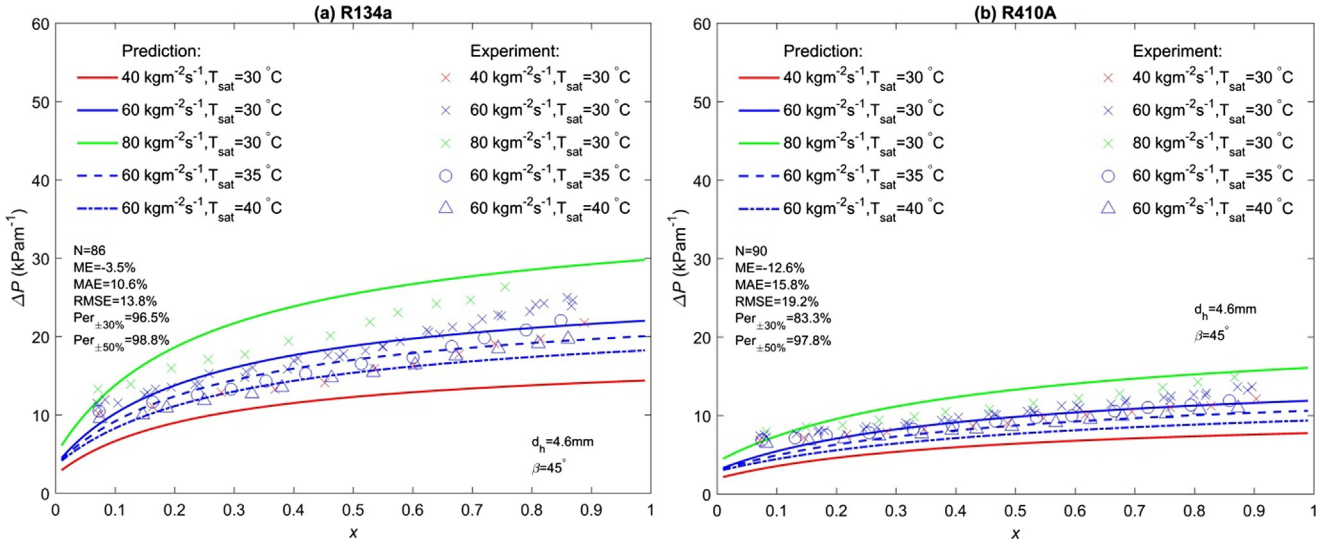

Fig. 5. Validation of the new frictional pressure drop correlation, Eq. (80), with the experimental data of (a) Park and Kim [65], (b) Park et al. [66].

mental data of large chevron angles, and under-predicts small chevron angles. The data of Winkelmann [15] are significantly under-predicted because of the small chevron angle. The correlation of Hayes et al. [37] over-predicts a large portion of the experimental data in Fig. 3(c).

In Fig. 3(d), Amalfi et al. [9] predicts 52.7% of the data within ±50%, which is relatively good. This correlation agrees well with the experimental database of evaporation and adiabatic processes. The gradient of vapor quality is opposite during evaporation and condensation.

In Fig. 3(e) and (f), the correlations of Winkelmann [15] and Nilpueng and Wongwises [63] generally under-predict the experimental data. Nilpueng and Wongwises [63] modified the original Lockhart-Martinelli model. Some of the predicted values decrease with the increasing experimental data of Yan et al. [20], Kuo et al. [16] and Winkelmann [15].

8. A new frictional pressure drop correlation

The prediction of frictional pressure drop is poor compared with heat transfer. This section develops a new frictional pressure drop correlation using multi-variable regression analysis. The shear force is assumed to rely on mass flux, vapor quality, heat flux, con-

densation pressure, fluid properties and plate geometries [4]. These influencing factors are expressed using the non-dimensional numbers listed in Section 2: X_{tt}, Co, Re_{eq}, Re_L, Re_{LO}, Re_G, We_{homo}, We_L, Fr_L, j_G, Bd, Bo, P_{sat}/P_{cr} and β.

The two-phase Fanning friction factor is derived from the experimental database. As shown in Eq. (79), the power law is chosen as the fitting mode by implementing least square method. Θ stands for non-dimensional numbers, and k_i, m_i and n_i are determined. Re_{eq}, Bd, P_{sat}/P_{cr} and β are found to be dominant. The inclusion of other numbers does not further improve the predicting accuracy. The resulting correlation is given in Eq. (80), where β is expressed in radian.

$$f_{TP} = \prod_{i=1}^{n} \left(k_i \Theta_i^{m_i} + n_i\right) \tag{79}$$

$$f_{TP} = \left(4.207 - 2.673\beta^{-0.46}\right)\left(4200 - 5.41Bd^{1.2}\right)Re_{eq}^{-0.95}\ \left(P_{sat}/P_{cr}\right)^{0.3} \tag{80}$$

Fig. 4 compares Eq. (80) with the experimental data. 87.5% of the data are predicted within ±50%, and the mean absolute error (MAE) is 31.2%. Since Eq. (80) is derived from the database, it is reasonable that the performance is much better than the other correlations shown in Fig. 3. This correlation is suitable in the operating ranges covered by Table 1. Eq. (80) is developed assuming homogeneous flow, and shows satisfactory prediction. In fact, more than one flow pattern may prevail, and a mechanistic model can be built considering the transition of flow patterns.

Fig. 5 validates the new correlation with experimental data that are not involved in the previous discussion. These experimental data were obtained in an oblong SPHE [65,66]. Although the top and bottom of the oblong plates are semi-circular, the main heat transfer area is rectangular and can be compared with traditional PHEs. Frictional pressure drop increases with mass flux and vapor quality, and the prediction follows the trend closely. Though the frictional pressure drop of small mass fluxes are underestimated, most of these experimental data are predicted within ±30%. The MAE is 10.6% for R134a and 15.8% for R410A. Additionally, the frictional pressure drop is larger for lower condensation temperature or lower reduced pressure. In this case, the fluid properties of liquid and vapor show larger differences, and the shear force between the two phases is stronger. The varying heat flux of the experimental data is not considered during the prediction, which has negligible influences. Nevertheless, the new correlation is not applicable for circular SPHEs, and under-predicts the experimental data significantly [25]. The circular plates change the flow passage area along the flow direction.

Fig. 6 is a sensitivity analysis, and the frictional pressure drop increases nearly linearly with mass flux. According to Fig. 6(a), R410A has the smallest frictional pressure drop. It is a high pressure refrigerant with the largest vapor density, which reduces the shear force at the two-phase interface. The frictional pressure drop of R601 is the largest. Fig. 6(b) shows the dependence on geometries. For smaller hydraulic diameter with narrower channel, the flow tends to be confined by the walls, and the corrugation structures promote the disturbance. Larger chevron angles enhance the secondary flow and intensify the stirring [67,68]. As a consequence, the frictional pressure drop is increased.

During condensation experiment, the overall pressure drop of PHEs, ΔP_{mea}, is measured directly. It is composed of frictional pressure drop, ΔP_{fri}, the pressure drop of inlet and outlet ports, ΔP_{in_port}, ΔP_{out_port}, deceleration pressure rise, ΔP_{de}, and elevation pressure rise, ΔP_{ele}. Eq. (81) calculates the frictional pressure drop as the flow passes the channels. The pressure drop of inlet and outlet ports is mostly obtained using empirical correlations. Although the port pressure drop accounts for a small portion of the overall value, these empirical correlations introduce unknown errors into the experimental frictional pressure drop, and should be validated depending on the port structures. The frictional pressure drop is contributed by three parts: inlet distributing region, fully developed region and outlet distributing region. Some of the PHEs have triangular inlet and outlet areas, where the fluid can be better distributed. This structure is common for GPHEs [15,69]. The inlet and outlet ports of BPHEs are mostly connected with rectangular areas directly [58,39].

$$\Delta P_{fri} = \Delta P_{mea} - \Delta P_{in\_port} - \Delta P_{out\_port} + \Delta P_{de} + \Delta P_{ele} \tag{81}$$

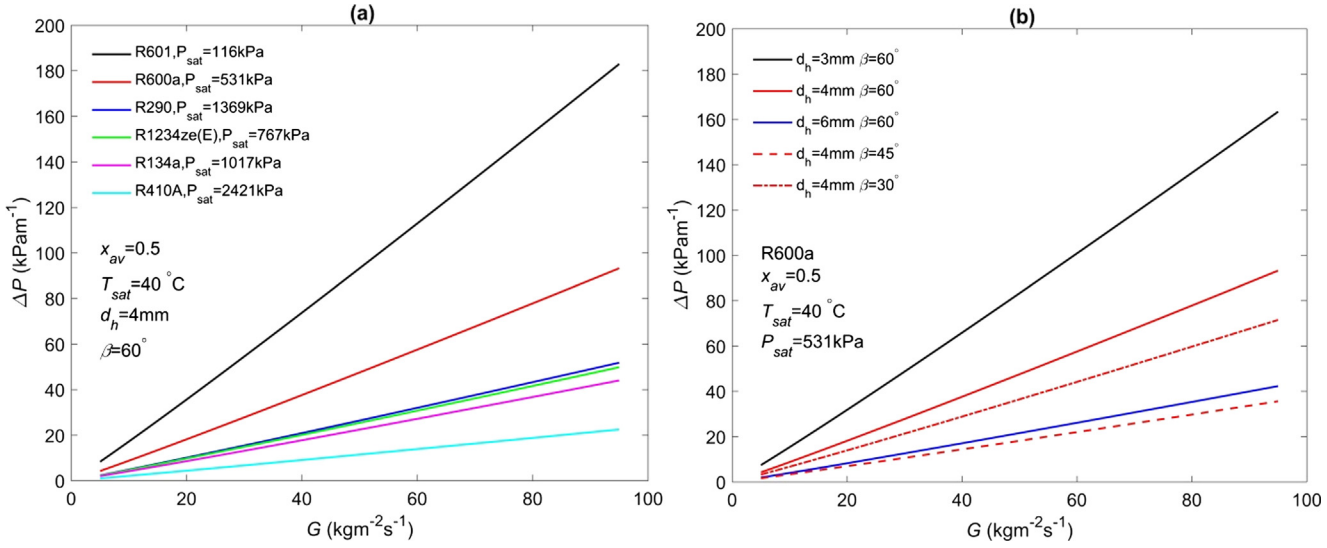

Fig. 6. Sensitivity of frictional pressure drop with mass flux for (a) different refrigerants, (b) different hydraulic diameter and chevron angle.

9. Conclusions

This paper investigates the predicting methods for heat transfer and frictional pressure drop during condensation in PHEs. The main conclusions are:

- An experimental database of condensation is built, which includes 2376 heat transfer data and 1590 frictional pressure drop data. The composition of the database is presented in terms of working fluids, chevron angles, hydraulic diameters, mass fluxes, saturated temperatures and reduced pressures.
- Heat transfer correlations are surveyed and are classified according to the basic forms. Eight heat transfer correlations are compared with the database. The correlations of Longo et al. [48] and Kuo et al. [16] predict 93.0% and 88.4% of the data within ±50%, respectively.
- Frictional pressure drop correlations are also reviewed. Six correlations are assessed with the database but show relatively poor performance. Thus a new correlation is developed, with 87.5% of the data predicted within ±50%. A cross validation shows good performance. A sensitivity analysis is provided for a wide range.

Suitable methods are presented to calculate the heat transfer and frictional pressure drop for the operating conditions covered by the experimental database. Although the database needs to be further extended such as to include NH_3 and wider ranges of vapor qualities, the presented methods are reliable for most refrigerants, various geometries, the reduced pressures below 0.5, as well as small and intermediate mass fluxes that are commonly used.

Conflict of interest

None.

Acknowledgements

This project has been developed in cooperation with Bluerise BV. The authors acknowledge the financial support from the China Scholarship Council and from the Koude Groep Delft/Wageningen. The authors are grateful for the contributions of Stijn van der Ploeg, Jasper Krombeen, Iram Saeed and Scott Heijerman from TU Delft.

References

[1] S. Jin, P. Hrnjak, A new method to simultaneously measure local heat transfer and visualize flow boiling in plate heat exchanger, Int. J. Heat Mass Transf. 113 (2017) 635–646.
[2] H.J. Kim, L. Liebenberg, A.M. Jacobi, Convective boiling of R-134a near the micro-macroscale transition inside a vertical brazed plate heat exchanger, J. Heat Transf. 140 (2018) 091501.
[3] M. Wang, C.A. Infante Ferreira, Absorption heat pump cycles with NH3 – ionic liquid working pairs, Appl. Energy 204 (2017) 819–830.
[4] X. Tao, M.P. Nuijten, C.A. Infante Ferreira, Two-phase vertical downward flow in plate heat exchangers: flow patterns and condensation mechanisms, Int. J. Refrig. 85 (2018) 489–510.
[5] B. Thonon, R. Vidil, C. Marvillet, Recent research and developments in plate heat exchangers, J. Enhanc. Heat Transf. 2 (1995) 149–155.
[6] J.R. García-Cascales, F. Vera-García, J.M. Corberán-Salvador, J. Gonzálvez-Maciá, Assessment of boiling and condensation heat transfer correlations in the modelling of plate heat exchangers, Int. J. Refrig. 30 (2007) 1029–1041.
[7] W.W. Akers, H.A. Deans, O.K. Crosser, Condensing heat transfer within horizontal tubes, Chem. Eng. Progr. 54 (1958) 89–90.
[8] R.L. Amalfi, F. Vakili-Farahani, J.R. Thome, Flow boiling and frictional pressure gradients in plate heat exchangers. Part 1: review and experimental database, Int. J. Refrig. 61 (2016) 166–184.
[9] R.L. Amalfi, F. Vakili-Farahani, J.R. Thome, Flow boiling and frictional pressure gradients in plate heat exchangers. Part 2: comparison of literature methods to database and new prediction methods, Int. J. Refrig. 61 (2016) 185–203.
[10] F. Vakili-Farahani, R.L. Amalfi, J.R. Thome, Two-phase heat transfer and pressure drop within plate heat exchangers, in: Encyclopaedia of Two-phase Heat Transfer and Flow II: Special Topics and Applications, 2016, pp. 145–215 (Chapter 4).
[11] R. Eldeeb, V. Aute, R. Radermacher, A survey of correlations for heat transfer and pressure drop for evaporation and condensation in plate heat exchangers, Int. J. Refrig. 65 (2016) 12–26.
[12] R.W. Lockhart, R.C. Martinelli, Proposed correlation of data for isothermal two-phase, two-component flow in pipes, Chem. Eng. Prog. 45 (1949) 39–48.
[13] J. Winkler, J. Killion, S. Garimella, B.M. Fronk, Void fractions for condensing refrigerant flow in small channels: Part I literature review, Int. J. Refrig. 35 (2012) 219–245.
[14] M.M. Shah, A new correlation for heat transfer during boiling flow through pipes, ASHRAE Trans. 82 (1976) 66–86.
[15] D. Winkelmann, Condensation of Pure Refrigerants and their Zeotropic Mixtures in Plate Heat Exchangers Ph.D. thesis, Commissiariat à l'energie atomique (CEA), 2010.
[16] W.S. Kuo, Y.M. Lie, Y.Y. Hsieh, T.F. Lin, Condensation heat transfer and pressure drop of refrigerant R-410A flow in a vertical plate heat exchanger, Int. J. Heat Mass Transf. 48 (25) (2005) 5205–5220.
[17] A. Jokar, M.H. Hosni, S.J. Eckels, Dimensional analysis on the evaporation and condensation of refrigerant R-134a in minichannel plate heat exchangers, Appl. Therm. Eng. 26 (2006) 2287–2300.
[18] J. Zhang, M.R. Kærn, T. Ommen, B. Elmegaard, H. Fredrik, Condensation heat transfer and pressure drop characteristics of R134a, R1234ze (E), R245fa and R1233zd (E) in a plate heat exchanger, Int. J. Heat Mass Transf. 128 (2019) 136–149.
[19] S.C. Palmer, W.V. Payne, P.A. Domanski, Evaporation and condensation heat transfer performance of flammable refrigerants in a brazed plate heat exchanger, NIST Report 6541 (2000).
[20] Y.-Y. Yan, H.-C. Lio, T.-F. Lin, Condensation heat transfer and pressure drop of refrigerant R-134a in a plate heat exchanger, Int. J. Heat Mass Transf. 42 (1999) 993–1006.
[21] Z.Y. Shi, J.P. Chen, V. Grabenstein, S. Kabelac, Experimental investigation on condensation heat transfer and pressure drop of R134a in a plate heat exchanger, Heat Mass Transf. 46 (2010) 1177–1185.
[22] B.H. Shon, C.W. Jung, O.J. Kwon, C.K. Choi, Y.T. Kang, Characteristics on condensation heat transfer and pressure drop for a low GWP refrigerant in brazed plate heat exchanger, Int. J. Heat Mass Transf. 122 (2018) 1272–1282.
[23] Z.Z. Wang, Z.N. Zhao, Analysis of performance of steam condensation heat transfer and pressure drop in plate condensers, Heat Transf. Eng. 14 (1993) 32–41.
[24] N. Hayes, A. Jokar, Z.H. Ayub, Study of carbon dioxide condensation in chevron plate exchangers; heat transfer analysis, Int. J. Heat Mass Transf. 54 (2011) 1121–1131.
[25] J. Lim, S.S. Kang, D. Kim, D.C. Lee, Y. Kim, Condensation heat transfer characteristics of R245fa in a shell and plate heat exchanger for high-temperature heat pumps, Int. J. Heat Mass Transf. 127 (2018) 730–739.
[26] K. Sarraf, S. Launay, G. El Achkar, L. Tadrist, Local vs global heat transfer and flow analysis of hydrocarbon complete condensation in plate heat exchanger based on infrared thermography, Int. J. Heat Mass Transf. 90 (2015) 878–893.
[27] S. Kabelac, S.W. Freund, Local two-phase flow heat transfer in plate heat exchangers, in: ASME/JSME Thermal Engineering Heat Transfer Summer Conference, 2007, pp. 469–477.
[28] E.M. Djordjević, S. Kabelac, P.S. Šerbanović, Heat transfer coefficient and pressure drop during refrigerant R-134a condensation in a plate heat exchanger, Chem. Pap. 62 (2008) 78–85.
[29] V. Grabenstein, S. Kabelac, Experimental and theoretical analysis of the local condensation heat transfer in a plate heat exchanger, J. Phys. Conf. Ser. 395 (2012) 012169.
[30] B. Thonon, A. Bontemps, Condensation of pure and mixture of hydrocarbons in a compact heat exchanger: experiments and modelling, Heat Transf. Eng. 23 (2002) 3–17.
[31] G.A. Longo, Refrigerant R134a condensation heat transfer and pressure drop inside a small brazed plate heat exchanger, Int. J. Refrig. 31 (2008) 780–789.
[32] G.A. Longo, R410A condensation inside a commercial brazed plate heat exchanger, Exp. Therm. Fluid Sci. 33 (2009) 284–291.
[33] G.A. Longo, The effect of vapour super-heating on hydrocarbon refrigerant condensation inside a brazed plate heat exchanger, Exp. Therm. Fluid Sci. 35 (2011) 978–985.
[34] S. Mancin, D. Del Col, L. Rossetto, Partial condensation of R407C and R410A refrigerants inside a plate heat exchanger, Exp. Therm. Fluid Sci. 36 (2012) 149–157.
[35] S. Mancin, D. Del Col, L. Rossetto, Condensation of superheated vapour of R410A and R407C inside plate heat exchangers: experimental results and simulation procedure, Int. J. Refrig. 35 (2012) 2003–2013.
[36] S. Mancin, D. Del Col, L. Rossetto, R32 partial condensation inside a brazed plate heat exchanger, Int. J. Refrig. 36 (2013) 601–611.
[37] N. Hayes, A. Jokar, Z.H. Ayub, Study of carbon dioxide condensation in chevron plate exchangers; pressure drop analysis, Int. J. Heat Mass Transf. 55 (2012) 2916–2925.
[38] P. Hrnjak, C. Kondou, Refrigerant side heat transfer in condensers with round tubes, Proceedings of the 4th IIR Conference on Thermophysical Properties and Transfer Processes of Refrigerants, Delft, The Netherlands, paper TP-087, 2013.
[39] K. Sarraf, S. Launay, L. Tadrist, Analysis of enhanced vapor desuperheating during condensation inside a plate heat exchanger, Int. J. Therm. Sci. 105 (2016) 96–108.

[40] J. Xiao, P. Hrnjak, Heat transfer and pressure drop of condensation from superheated vapor to subcooled liquid, Int. J. Heat Mass Transf. 103 (2016) 1327–1334.
[41] J. Xiao, P. Hrnjak, A new flow regime map and void fraction model based on the flow characterization of condensation, Int. J. Heat Mass Transf. 108 (2017) 443–452.
[42] E.W. Lemmon, M.L. Huber, M.O. McLinden, NIST Standard Reference Database 23: Reference Fluid Thermodynamic and Transport Properties-REFPROP, Version 9.1, National Institute of Standards and Technology, Standard Reference Data Program, Gaithersburg, 2013.
[43] J.S. Brown, C. Zilio, A. Cavallini, The fluorinated olefin R-1234ze(Z) as a high-temperature heat pumping refrigerant, Int. J. Refrig. 32 (2009) 1412–1422.
[44] R.J. Hulse, R.S. Basu, R.R. Singh, R.H.P. Thomas, Physical properties of HCFO-1233zd (E), J. Chem. Eng. Data 57 (2012) 3581–3586.
[45] C. Kondou, R. Nagata, N. Nii, S. Koyama, Y. Higashi, Surface tension of low GWP refrigerants R1243zf, R1234ze (Z), and R1233zd (E), Int. J. Refrig. 53 (2015) 80–89.
[46] G. Raabe, Molecular simulation studies on the vapor–liquid equilibria of the cis-and trans-HCFO-1233zd and the cis-and trans-HFO-1336mzz, J. Chem. Eng. Data 60 (2015) 2412–2419.
[47] W. Nusselt, Die Oberflachenkondensation des Wasserdampfes, Z. Ver. D. Ing. 60 (1916) 541–546.
[48] G.A. Longo, G. Righetti, C. Zilio, A new computational procedure for refrigerant condensation inside herringbone-type Brazed Plate Heat Exchanger, Int. J. Heat Mass Transf. 82 (2015) 530–536.
[49] R.L. Webb, Convective condensation of superheated vapor, J. Heat Transf. 120 (2) (1998) 418–421.
[50] D.H. Han, K.J. Lee, Y.H. Kim, The characteristics of condensation in brazed plate heat exchangers with different chevron angles, J. Korean Phys. Soc. 43 (2003) 66–73.
[51] J. Soontarapiromsook, O. Mahian, A.S. Dalkilic, S. Wongwises, Effect of surface roughness on the condensation of R-134a in vertical chevron gasketed plate heat exchangers, Exp. Therm. Fluid Sci. 91 (2018) 54–63.
[52] R. Würfel, N. Ostrowski, Experimental investigations of heat transfer and pressure drop during the condensation process within plate heat exchangers of the herringbone-type, Int. J. Therm. Sci. 43 (2004) 59–68.
[53] M.M. Shah, A general correlation for heat transfer during film condensation inside pipes, Int. J. Heat Mass Transf. 22 (1979) 547–556.
[54] A. Cavallini, D.D. Col, L. Doretti, M. Matkovic, L. Rossetto, C. Zilio, G. Censi, Condensation in horizontal smooth tubes: a new heat transfer model for heat exchanger design, Heat Transf. Eng. 27 (2006) 31–38.
[55] L. Silver, Gas cooling with aqueous condensation, Trans. Inst. Chem. Eng. 25 (1947) 30–42.
[56] K.J. Bell, M.A. Ghaly, An approximate generalized design method for multicomponent/partial condenser, AIChE Symp. 39 (1972) 72–79.
[57] P. Stephan, H. Martin, S. Kabelac, D. Mewes, M. Kind, K. Schaber, VDI Heat Atlas, second ed., Springer, Dusseldorf, 2010.
[58] G.A. Longo, Heat transfer and pressure drop during HFC refrigerant saturated vapour condensation inside a brazed plate heat exchanger, Int. J. Heat Mass Transf. 53 (2010) 1079–1087.
[59] G.A. Longo, Heat transfer and pressure drop during hydrocarbon refrigerant condensation inside a brazed plate heat exchanger, Int. J. Refrig. 33 (2010) 944–953.
[60] M.K. Dobson, J.C. Chato, Condensation in smooth horizontal tubes, ASME J. Heat Transf. 120 (1998) 193–213.
[61] J.R. Thome, J. El Hajal, A. Cavallini, Condensation in horizontal tubes, part 2: new heat transfer model based on flow regimes, Int. J. Heat Mass Transf. 46 (2003) 3365–3387.
[62] D. Chisholm, A theoretical basis for the Lockhart-Martinelli correlation for two-phase flow, Int. J. Heat Mass Transf. 10 (1967) 1767–1778.
[63] K. Nilpueng, S. Wongwises, Two-phase gas-liquid flow characteristics inside a plate heat exchanger, Exp. Therm. Fluid Sci. 34 (2010) 1217–1229.
[64] E.W. Jassim, T.A. Newell, J.C. Chato, Refrigerant pressure drop in chevron and bumpy style flat plate heat exchangers, Exp. Therm. Fluid Sci. 30 (2006) 213–222.
[65] J.H. Park, Y.S. Kim, Condensation Heat Transfer and Pressure Drop of R-134a in the Oblong Shell and Plate Heat Exchanger, Int. J. Air-Cond. Refrig. 12 (2004) 158–167.
[66] J.H. Park, Y.H. Kwon, Y.S. Kim, Experimental study on R-410A condensation heat transfer and pressure drop characteristics in oblong shell and plate heat exchanger, International Refrigeration and Air Conditioning Conference. Purdue, America, 2004.
[67] K. Sarraf, S. Launay, L. Tadrist, Complex 3D-flow analysis and corrugation angle effect in plate heat exchangers, Int. J. Therm. Sci. 94 (2015) 126–138.
[68] H.B. Luan, J.P. Kuang, Z. Cao, Z. Wu, W.Q. Tao, B. Sundén, CFD analysis of two types of welded plate heat exchangers, Numer. Heat Transf. Part A 71 (2017) 250–269.
[69] X. Tao, E. Dahlgren, C. Infante Ferreira, Local NH3 condensation in a plate heat exchanger, 13th IIR Gustav Lorentzen Conference on Natural Refrigerants. Valencia, Spain, 2018.
[70] G.A. Longo, C. Zilio, Condensation of the low GWP refrigerant HFC1234yf inside a brazed plate heat exchanger, Int. J. Refrig. 36 (2) (2013) 612–621.
[71] G.A. Longo, C. Zilio, G. Righetti, J.S. Brown, Condensation of the low GWP refrigerant HFO1234ze(E) inside a Brazed Plate Heat Exchanger, Int. J. Refrig. 38 (2014) 250–259.
[72] G.A. Longo, C. Zilio, G. Righetti, J.S. Brown, Experimental assessment of the low GWP refrigerant HFO-1234ze (Z) for high temperature heat pumps, Exp. Therm. Fluid Sci. 57 (2014) 293–300.
[73] G.A. Longo, C. Zilio, G. Righetti, Condensation of the low GWP refrigerant HFC152a inside a brazed plate heat exchanger, Exp. Therm. Fluid Sci. 68 (2015) 509–515.
[74] G.A. Longo, S. Mancin, G. Righetti, C. Zilio, HFC404A condensation inside a small brazed plate heat exchanger: comparison with the low GWP substitutes propane and propylene, Int. J. Refrig. 81 (2017) 41–49.